공학석사학위논문

유연 시스템의 모델 프리 최적 추정 및 센서 배치 프레임워크 개발

Model-Free Optimal Estimation and Sensor Placement Framework for Elastic Kinematic Chain

2019 년 2 월

서울대학교 대학원

기계항공공학부

안 준 모

Abstract

Model-Free Optimal Estimation and Sensor Placement Framework for Elastic Kinematic Chain

Joonmo Ahn
Mechanical & Aerospace Engineering
The Graduate School
Seoul National University

In this thesis, we propose a novel model-free optimal estimation and sensor placement framework for a high-DOF (degree-of-freedom) EKC (elastic kinematic chain) with only a limited number of IMU (inertial measurement unit) sensors based on POD (proper orthogonal decomposition) and MAP (maximum a posteriori) estimation. First, we (off-line) excite the system richly enough, collect the data and perform the POD to extract dominant and non-dominant modes. We then decide the minimum number of IMUs according to the dominant modes, and construct the prior distribution of the output (i.e., top-end position of EKC) based on the singular value of each POD mode. We also formulate the MAP estimation given the prior distribution and different placements of the IMUs and choose the optimal IMU placement to maximize the posterior probability. This optimal placement is then used for real-time output estimation of the EKC. Experiments are also performed to verify the theory.

Keywords: Elastic kinematic chain, Proper orthogonal decomposition, Proper orthogonal mode, Mode reduction, Maximum a posteriori estimation, Sensor placement optimization
Student Number: *2017-28758*

Acknowledgements

짧은 듯 길었던 2년이 지나가고, 또 다시 겨울이 돌아와 졸업을 앞둔 이 시점에서 지난 2년을 되돌아봅니다. 미숙하기만 했던 신입생 시절과 비교해보면, 대학원에서 많은 경험과 추억을 얻어 더 발전된 공학도로 졸업하게 되어 뿌듯합니다.

우선 석사과정 생활 동안 아낌없는 가르침을 주신 이동준 교수님께 감사의 말씀을 드립니다. 학문을 대하는 태도에 있어서 항상 이유를 제시할 수 있어야 하고, 엄밀함을 추구하는 자세를 교수님으로부터 배울 수 있었습니다. 또한, 학생들의 말에도 귀기울여 들으려고 노력하시는 모습은 학자로서뿐만 아니라 인생 선배로서도 본받을 점이 많았습니다. 교수님으로부터 배운 학문과 삶을 대하는 태도는 대학원을 졸업하고 새로운 삶의 여정을 시작하며 훌륭한 밑거름이 될 것이라 생각합니다.

대학원 생활을 하며 얻은 가장 큰 자산 중 하나는 훌륭한 동료들입니다. 항상 열정적이며, 서로 도울 줄 알며, 인생의 즐거움 또한 잊지 않는 든든한 INRoL 동료들이 있었기에 보람찬 대학원 생활을 보낼 수 있었습니다. 함께 2년을 동고동락한 창수, 뉴엔, 명신, 현수, 상율, 용석, 재민, 광민, 호용, 창우, 상윤, 용준, 준영, 학찬, 정섭, 민지, 용한, 락준, 효준, 성진, 동원, 부건, 후창, 창묵, 일권, 원하 모두에게 감사의 인사드립니다.

그리고 항상 저를 응원해주신 아버지, 어머니, 그리고 누나들에게 감사의 말씀 전합니다. 가족들의 사랑 덕분에 대학원 생활을 성공적으로 마무리할 수 있었습니다.

2019년 1월

안준모

Contents

List of Figures

List of Tables

Abbreviations

EKC	**E**lastic **K**inematic **C**hain
DOF	**D**egree **o**f **F**reedom
POD	**P**roper **O**rthogonal **D**ecomposition
POM	**P**roper **O**rthogonal **M**ode
PCA	**P**rincipal **C**omponent **A**nalysis
IMU	**I**nertial **M**easurement **U**nit
FBG	**F**iber **B**ragg **G**rating
MAP	**M**aximum **a** **P**osteriori
RMS	**R**oot **M**ean **S**quare

Chapter 1

Introduction

This thesis is motivated by the problem of how to estimate the mast top-end motion (or deflection at the stage) of the telerobotic system as shown in Fig. 1.1, which consists of a telescoping mast of about ten-meter high, a stage with planar actuation (i.e., SE(2)) and two industrial manipulators on top of the stage. This telerobotic system is developed for nuclear power plant maintenance operations at height. One of the key issues for this telerobotic system is how to allow a remote user to teleoperate the end-effector of the manipulators while suppressing the mast vibration, which is induced in turn by the motion of the manipulators (and the stage). More details on this telerobotic system and the control framework of simultaneous manipulator tracking and mast vibration suppression are analyzed in [1].

For this mast vibration suppression feedback control, it is necessary to estimate the mast top-end motion (i.e., just beneath the stage). This is achieved with MOCAP (motion capture) system in [1]. Such external sensors, however, are not assumable for typical nuclear plant environments due to radiation and onboard sensing strategy is demanded. For this onboard mast top-end motion estimation come with the following technical challenges: 1) the mast is a high-DOF (degree-of-freedom) system (e.g., ten-link mast in Fig. 1.1 modeled as a twenty-DOF system with universal joints), thus, in many cases, it is infeasible to deploy that many sensors to measure all its DOFs, and, further, the behavior of mast is usually "reducible" with some dominant modes as long as the system and the control are designed reasonably-well; 2) the mast has high-DOF complicated/nonlinear kinematics and dynamics, thus, often, it is difficult to identify those many system parameters (e.g., stiffness, mass, damping, etc.) and solve the high-DOF kinematic/dynamic equations as accurately and quickly as to be useful for the vibration suppression control; and 3) due to the implementation cost, effort and complexity, it is typically desired (or, often, necessary) to minimize the number of deployed sensors as much as possible while still ensuring the estimation performance.

To address these challenges, in this thesis, we propose a novel model-free/data-driven optimal estimation and sensor placement framework for this high-DOF mast based on mode reduction via proper orthogonal decomposition (POD) [2, 3] and maximum a posteriori (MAP) estimation [4]. For this, we first model the telescoping mast as an EKC (elastic kinematic chain) system [5] with each segment

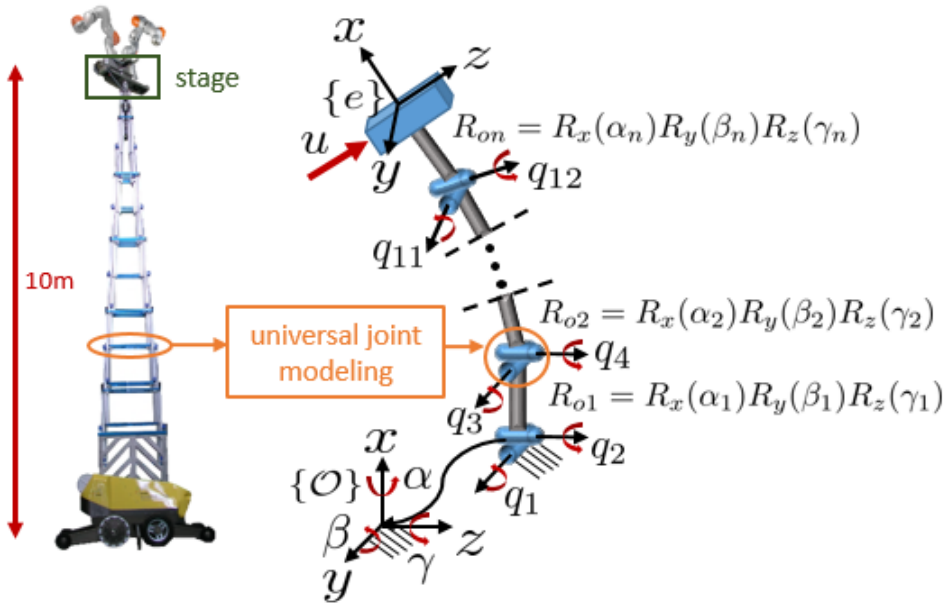

FIGURE 1.1: Telescoping mast and n-link three-dimensional elastic kinematic chain system with universal joints with torsional spring and damper.

connected via an universal joint (with pitch, yaw, roll angles) with each other (see Fig. 1.1). We also adopt IMUs (inertial measurement units with compass) as onboard sensors due to their high speed, low cost, easy implementation, ability to measure all three-DOF rotations by one sensor, and availability of many standard algorithms to process its signal (e.g., [6, 7]). Our framework then proceeds according to the following orders:

(1) Excite the mast emulating the whole spectrum of "representative" operations, collect the angle data of all the segments, and perform POD to

decompose system behavior into dominant and non-dominant modes;

(2) Decide the minimum number of IMUs according to the number of dominant modes, and construct prior distribution of the output (i.e., mast top-end motion) with each mode assumed to be excited by zero-mean Gaussian with its variance proportional to the mode singular value of POD;

(3) Compute MAP given the prior distribution and different placement of the given number of IMUs (with their sensing uncertainty), choose the optimal placement of IMUs to optimize this MAP estimation,

(4) Real-time estimate the mast top-end motion by using the IMUs optimally placed as decided above and the prior distribution of the output.

Here, note that: 1) the steps (1)-(3) are performed off-line, whereas the step (4) on-line; 2) the framework is model-free, as it does not utilize any (complex) dynamics model and its (difficult-to-identify) parameters; and 3) validity of (linear) mode reduction via POD is granted with the suitably-functioning vibration suppression control of [1]. This framework would be applicable to similar setups (e.g., continuum manipulators [8]) with different sensors as well (e.g., low-rate camera, limited-accuracy range-finder, etc.).

Many results have been proposed for this motion/shape estimation problem of EKC systems. Vision-based shape estimation techniques are presented in [9–11], yet, the cameras as used there are typically much slower (around 20Hz) than the IMUs (200Hz) and often need to be mounted externally, thus, not so suitable for

the vibration suppression control as compared to the IMUs. The scheme of [12] allow for the configuration estimation of the EKC with a single electromagnetic sensor, yet, requires to real-time solve the equilibrium of the high-DOF quasi-static equation of the EKC. Shape reconstruction techniques for flexible structure using Fiber Bragg Grating (FBG) sensors are studied in [13, 14], yet, those FBG sensors are typically much more expensive to implement for the large-size as our mast system with powerful transmitters and boosters necessitated. A novel framework of model-free optimal output estimation and sensor placement for a large-size high-DOF EKC system is proposed in [15]. On the extension of [15], this thesis includes experiment result of large-size mock-up.

The rest of the thesis is organized as follows. Chapter 2 presents the EKC modeling of the mast system and problem statement. Chapter 3 explains our proposed framework, consisting of mode reduction approach with POD, optimal estimation formulation via maximum a posteriori estimation and optimal sensor placement based on that. In Chapter 4, we verify our framework via experiments executed with a small-scale six-link EKC testbed and large-size mock-up. Finally, in Chapter 5, we conclude the thesis with summary and comments on future research.

Chapter 2

System Modeling and Problem Statement

2.1 System Modeling

In this thesis, we consider n-link EKC system, where each link is connected by elastic components such as torsional spring and damper. Each joint is modeled as universal joint, where two-DOF rotational motion is possible. See Fig. 1.1, where spatial rotation of each joint is described by relative joint angles of each universal joint $q(t) \in \Re^{2n}$. The same motion also can be expressed with $\phi_i(t) := [\alpha_i(t), \beta_i(t), \gamma_i(t)]^T \in \Re^3$, where $\alpha_i(t)$, $\beta_i(t)$, $\gamma_i(t) \in \Re$ are roll, pitch, and yaw

angles of i-th link w.r.t. global frame $\{\mathcal{O}\}$. Then, we define total configuration state $\phi(t) := [\phi_1^T(t), \phi_2^T(t), \cdots, \phi_n^T(t)]^T \in \Re^{3n}$.

We may express dynamics and output of the system as following nonlinear equation

$$\begin{bmatrix} \ddot{\phi}(t) \\ \dot{\phi}(t) \end{bmatrix} = f\left(\begin{bmatrix} \dot{\phi}(t) \\ \phi(t) \end{bmatrix}, u(t) \right), \quad \psi(t) = h(\phi(t)) \tag{2.1}$$

where $u(t) \in \Re^p$ and $\psi(t) \in \Re^s$, respectively, denote the input (e.g., external force), and output of the system. The output $\psi(t)$ can be defined arbitrarily depending on what user thinks as important factor for scenario (e.g., top-end motion). We constrain the output $\psi(t)$ to be function of the configuration state $\phi(t)$ for simplicity.

2.2 Problem Statement

Objective of this thesis is to estimate the output of the EKC system. However, following technical challenges exist:

- system parameters are difficult to obtain, hence real-time dynamics computation may not be feasible or not accurate
- deploying sensors on every link may not be feasible due to high-DOF of the system, or practical implementation issue

In this thesis, we propose an optimal output estimation and sensor placement framework for EKC, given the limited number of practically implementable sensors. We use IMU sensors since the state of the system can be measured utilizing explicit nonlinear complementary filter [7].

Chapter 3

Optimal Estimation and Sensor Placement

3.1 Output Estimation

3.1.1 Linearization

We assume small deviation of the state with the vibration suppression control proposed in [1]. Therefore, we focus on linearized approach near the steady-state.

Then, we can approximate the output equation from (2.1) as

$$\tilde{\psi}(t) \approx \underbrace{\left.\frac{\partial h}{\partial \phi}\right|_{\phi=\phi_{ss}}}_{=:\hat{S}} \tilde{\phi}(t) \tag{3.1}$$

where $\tilde{\psi}(t) \in \Re^s$ and $\tilde{\phi}(t) \in \Re^{3n}$, respectively, denote the output and the state deviation from their steady-state. $\hat{S} \in \Re^{s\times 3n}$ is state-output linear relationship matrix. It can be obtained either analytically or by regression if ground-truth value of the output is available. The first method is straightforward if one knows perfect kinematics of the system. For second method , we need matrix optimization. If we apply sufficient excitation to the system and obtain measurement data of the output and the state, $\hat{S}$ is obtained from following matrix optimization:

$$\begin{aligned}
\hat{S} &= \underset{S}{\operatorname{argmin}} \sum_{k=1}^{N} \|\tilde{\psi}_k - S\tilde{\phi}_k\|_2^2 \\
&= \underset{S}{\operatorname{argmin}}\, \mathbf{tr}\left[\sum_{k=1}^{N} \tilde{\phi}_k^T S^T S \tilde{\phi}_k \; - 2\sum_{k=1}^{N} \tilde{\psi}_k^T S \tilde{\phi}_k\right] \\
&= \underset{S}{\operatorname{argmin}}\, \mathbf{tr}\left[\underbrace{\left(\sum_{k=1}^{N} \tilde{\phi}_k \tilde{\phi}_k^T\right)}_{=:X} S^T S - 2\underbrace{\left(\sum_{k=1}^{N} \tilde{\phi}_k \tilde{\psi}_k^T\right)}_{=:Y} S\right] \\
&= \underset{S}{\operatorname{argmin}}\, \mathbf{L}(S)
\end{aligned}$$

where $\mathbf{L}(S) := \mathbf{tr}(XS^TS - 2YS) \in \Re$. $\tilde{\psi}_k \in \Re^s$ and $\tilde{\phi}_k \in \Re^{3n}$, respectively, denote the output and the state data at time step t_k. Now, global minimum

of this optimization is obtained via solving $d\mathbf{L}_V(\hat{S}) = 0,\ {}^{\forall}V \in \Re^{s\times 3n}$, where $d\mathbf{L}_V(S)$ is defined as

$$\begin{aligned} d\mathbf{L}_V(S) &:= \lim_{\epsilon\to 0}\frac{1}{\epsilon}\left[\mathbf{L}(S+\epsilon V) - \mathbf{L}(S)\right] \\ &= \lim_{\epsilon\to 0}\frac{1}{\epsilon}\mathbf{tr}\left[X(S+\epsilon V)^T(S+\epsilon V) - 2Y(S+\epsilon V) - XS^TS + 2YS\right] \\ &= \mathbf{tr}\left[XS^TV + XV^TS - 2YV\right] \\ &= 2\ \mathbf{tr}\left[(XS^T - Y)V\right] \end{aligned}$$

Therefore, it is straightforward to obtain the global minimum

$$\hat{S} = Y^TX^{-T} = Y^TX^{-1}$$

From now on, we will call $\tilde{\phi}(t)$ as the "state" and $\tilde{\psi}(t)$ as the "output" of the system, omitting "deviation from steady-state" for convenience.

3.1.2 Mode Reduction

To cover wide variety of operation scenarios, let us assume the input is randomly applied to the system. Then, distribution of the state can be assumed as Gaussian, and its behavior can be decomposed into dominant modes and non-dominant modes. This decomposition is achieved by proper orthogonal decomposition (POD) [2]. The method is also known as principal component analysis (PCA) [16], Karhunen-Loeve method [17], and it is related to controllability

Gramian [18]. Then, this make us possible to choose minimum number of sensors according to the dominant modes.

Experimentally, we apply the input to the system, emulating the representative operations richly enough to cover whole spectrum of the system behavior. Then, obtain data of the state for sufficiently large time step. If we apply singular value decomposition to the state data covariance $C_\phi \in \Re^{3n\times 3n}$, we have

$$C_\phi = \frac{1}{N}\sum_{k=1}^{N} \tilde{\phi}_k \tilde{\phi}_k^T = U\Sigma U^T \tag{3.2}$$

where $\tilde{\phi}_k \in \Re^{3n}$ denotes the state at time step t_k. $\Sigma = \mathrm{diag}[\sigma_1, \sigma_2, \cdots, \sigma_{3n}] \in \Re^{3n\times 3n}$ is a diagonal matrix, whose singular values of C_ϕ are ordered in descending order, i.e., $\sigma_1 \geq \sigma_2 \geq \cdots \geq \sigma_{3n}$. In addition, column vectors of orthogonal matrix $U \in \Re^{3n\times 3n}$ are proper orthogonal modes (POMs), which are listed from dominant to non-dominant mode, of the system corresponding to its singular value. Then, we can express $\tilde{\phi}(t)$ as combinations of POMs:

$$\tilde{\phi}(t) = U\xi(t) \tag{3.3}$$

where $\xi(t) \in \Re^{3n}$ is transformed state.

From the result of POD, we can reduce the $3n$-dimensional state space into r-dimensional subspace that preserves most of the "energy" of the original state, which is known as model reduction [19, 20]. r can be chosen such that $\frac{\sum_{i=1}^{r}\sigma_i}{\sum_{i=1}^{3n}\sigma_i}$ is larger than certain threshold. It is known that matrix whose columns are

eigenvectors corresponding to first r greatest eigenvalues of C_ϕ is projection matrix that preserves most energy (2-norm) of the state in the r-dimensional subspace [19]. In other words, if we define projection matrix that projects the $3n$-dimensional state to r-dimensional subspace as $P \in \Re^{3n\times r}$ with r unit column vectors, we have following constrained optimization problem to obtain projection matrix P that preserves most of the 2-norm energy in r-dimensional subspace.

$$\underset{P}{\text{argmax}} \frac{1}{N}\sum_{k=1}^{N} \|\tilde{\phi}_k^T P\|_2^2 \qquad \text{subj. to } P_i^T P_i = 1,\ i \in \{1,\cdots,r\}$$

where $P_i \in \Re^{3n}$ denotes i-th column of P. Solution of this optimization problem is as follows using (3.2):

$$\begin{aligned}
&\underset{P}{\text{argmax}} \frac{1}{N}\sum_{k=1}^{N}\sum_{i=1}^{r} \left(\tilde{\phi}_k^T P_i\right)^2 + \sum_{i=1}^{r}\left[\lambda_i\left(1 - P_i^T P_i\right)\right] \\
=&\underset{P}{\text{argmax}} \frac{1}{N}\sum_{k=1}^{N}\sum_{i=1}^{r} P_i^T \tilde{\phi}_k \tilde{\phi_k}^T P_i + \sum_{i=1}^{r}\left[\lambda_i\left(1 - P_i^T P_i\right)\right] \\
=&\underset{P}{\text{argmax}} \sum_{i=1}^{r}\left[P_i^T C_\phi P_i + \lambda_i\left(1 - P_i^T P_i\right)\right]
\end{aligned}$$

Consequently, we have the solution

$$C_\phi P_i = \lambda_i P_i, \qquad i \in \{1,\cdots,r\}$$

This implies each column of P, which is P_i, is eigenvector of C_ϕ and Lagrange multiplier λ_i is its corresponding eigenvalue. Therefore we have

$$\max_P \frac{1}{N}\sum_{k=1}^{N}\|\tilde{\phi}_k^T P\|_2^2 = \max_P \sum_{i=1}^{r} P_i^T C_\phi P_i = \max_P \sum_{i=1}^{r}\lambda_i = \sum_{i=1}^{r}\sigma_i$$

This means to maximize the cost, or 2-norm energy of the state, we must choose r greatest eigenvalues, or first r greatest singular values of C_ϕ. Hence this leads to following solution of the optimization

$$U_1 = \underset{P}{\text{argmax}}\frac{1}{N}\sum_{k=1}^{N}\|\tilde{\phi}_k^T P\|_2^2 \qquad \text{subj. to } P_i^T P_i = 1,\ i \in \{1,\cdots,r\}$$

where $U_1 \in \Re^{3n\times r}$ is first r columns of U, which are eigenvectors corresponding to the first r greatest eigenvalues of C_ϕ. This implies that projection of the state to column space of U_1 preserves most of the 2-norm energy, and the maximum value of the energy is sum of the first r singular values of C_ϕ, which is $\sum_{i=1}^{r}\sigma_i$. In the same sense, projection matrix $P' \in \Re^{3n\times(3n-r)}$ that minimizes 2-norm energy of the state in $(3n-r)$-dimensional subspace is

$$U_2 = \underset{P'}{\text{argmin}}\frac{1}{N}\sum_{k=1}^{N}\|\tilde{\phi}_k^T P'\|_2^2 \qquad \text{subj. to } P_i'^T P_i' = 1,\ i \in \{1,\cdots,3n-r\}$$

where $U_2 \in \Re^{3n\times(3n-r)}$ is last $3n-r$ columns of U, which are eigenvectors corresponding to the $3n-r$ least eigenvalues of C_ϕ. And, the minimum value of

the energy is

$$\min_{P'} \frac{1}{N} \sum_{k=1}^{N} \|\tilde{\phi}_k^T P'\|_2^2 = \sum_{i=r+1}^{3n} \sigma_i$$

Then, let us decouple (3.3) into

$$\begin{aligned} \tilde{\phi}(t) = U\xi(t) &= [U_1 \; U_2] \begin{bmatrix} \xi_1(t) \\ \xi_2(t) \end{bmatrix} \\ &= U_1\xi_1(t) + U_2\xi_2(t) \end{aligned} \tag{3.4}$$

where $U_1 \in \Re^{3n \times r}$ and $U_2 \in \Re^{3n \times (3n-r)}$, respectively, are first r dominant POMs and $3n - r$ non-dominant POMs. $\xi_1(t) \in \Re^r$ and $\xi_2(t) \in \Re^{3n-r}$, respectively, are dominant transformed state and non-dominant transformed state. For convenience, we will call $\xi_1(t)$ as "dominant state" and $\xi_2(t)$ as "non-dominant state."

Since now we have the decoupled state (3.4), we can obtain covariance of the dominant state $\xi_1(t)$ and the non-dominant state $\xi_2(t)$ from (3.2). Substituting (3.4) into (3.2), we have

$$\begin{aligned} C_\phi &= \frac{1}{N} \sum_{k=1}^{N} \tilde{\phi}_k \tilde{\phi}_k^T \\ &= \frac{1}{N} \sum_{k=1}^{N} (U_1\xi_{1,k} + U_2\xi_{2,k})(U_1\xi_{1,k} + U_2\xi_{2,k})^T \end{aligned}$$

where $\xi_{1,k} \in \Re^r$ and $\xi_{2,k} \in \Re^{3n-r}$, respectively, denote $\xi_1(t)$ and $\xi_2(t)$ at time step t_k. Using orthonormal property of U,

$$U^T U = I_{3n\times 3n}$$
$$U_1^T U_1 = I_{r\times r}, \quad U_2^T U_2 = I_{(3n-r)\times(3n-r)}, \quad U_1^T U_2 = 0_{r\times(3n-r)}$$

it is straightforward to have

$$C_\phi = U_1 \underbrace{\left(\frac{1}{N}\sum_{k=1}^{N} \xi_{1,k}\xi_{1,k}^T\right)}_{=:C_{\xi_1}} U_1^T + U_2 \underbrace{\left(\frac{1}{N}\sum_{k=1}^{N} \xi_{2,k}\xi_{2,k}^T\right)}_{=:C_{\xi_2}} U_2^T \tag{3.5}$$

From (3.2), let us partition the diagonal matrix Σ into dominant part and non-dominant part

$$U^T C_\phi U = \begin{bmatrix} \Sigma_1 & 0 \\ 0 & \Sigma_2 \end{bmatrix} \tag{3.6}$$

where $\Sigma_1 \in \Re^{r\times r}$ is diagonal matrix with its elements composed of singular values of the dominant POMs and $\Sigma_2 \in \Re^{(3n-r)\times(3n-r)}$ is diagonal matrix with its elements composed of singular values of the non-dominant POMs. From (3.5), (3.6), and utilizing orthonormality of U, we have covariances of $\xi_1(t)$ and $\xi_2(t)$ as follows:

$$C_{\xi_1} = \Sigma_1, \quad C_{\xi_2} = \Sigma_2$$

If no information of measurements is given, we may assume the prior distributions of the state, the dominant state, and the non-dominant state as $\tilde{\phi}(t) \sim \mathcal{N}(0, C_\phi)$, $\xi_1(t) \sim \mathcal{N}(0, C_{\xi_1})$, and $\xi_2(t) \sim \mathcal{N}(0, C_{\xi_2})$, where $\mathcal{N}(\mu, C)$ denotes the Gaussian distribution of mean μ and covariance C. Note that, since the diagonal elements of Σ_2 are much smaller than those of Σ_1, we may say that the state space can be reduced to r-dimensional subspace composed of its dominant POMs, and assume the non-dominant state part as model noise term. In other words, $U_1\xi_1(t)$ in (3.4) is reduced state, and $U_2\xi_2(t)$ can be regarded as model noise. Thanks to POD, we are now able to choose number of sensors that give us at least more measurements than order of the dominant state r.

3.1.3 Maximum a Posteriori Estimation

Recall that our objective of this thesis is to estimate user-defined output $\tilde{\psi}(t)$ of the system. However, we only have some "part" of the measurement of the full state from IMUs. Therefore, we must reconstruct measurement of the output from the reduced state. Suppose measurement from IMUs are given by

$$y_\phi(t) = H\tilde{\phi}(t) + \nu(t) \in \Re^m, \quad \nu(t) \sim \mathcal{N}(0, C_\nu) \tag{3.7}$$

where $H \in \Re^{m\times 3n}$ is IMU placement matrix, $\nu(t) \in \Re^m$ is zero-mean Gaussian sensor noise with covariance $C_\nu \in \Re^{m\times m}$, and $m \leq 3n$. With the knowledge of the decomposed state into dominant and non-dominant part, substituting (3.4)

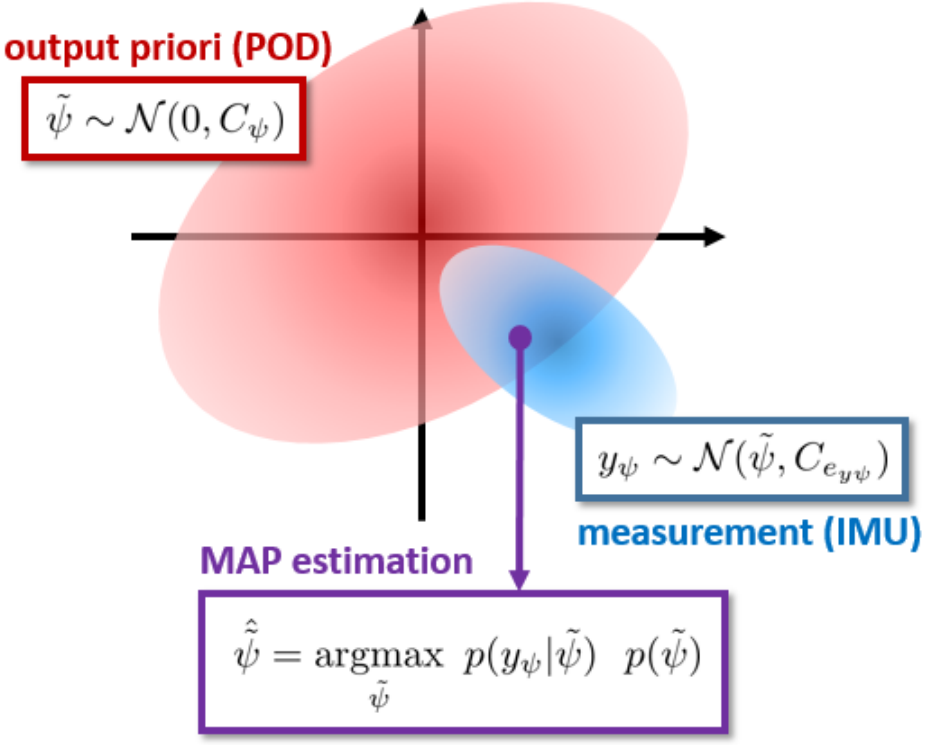

FIGURE 3.1: Maximum a posteriori estimation of output

into (3.7), we have

$$y_\phi(t) = \underbrace{HU_1}_{=:\tilde{U}_1}\xi_1(t) + \underbrace{HU_2}_{=:\tilde{U}_2}\xi_2(t) + \nu(t)$$

Now, assuming $\xi_2(t) \sim \mathcal{N}(0, C_{\xi_2})$ as noise term, we have least squares solution of $\xi_1(t)$ with $m \geq r$

$$\begin{aligned}\hat{\xi}_1 &= \underset{\xi_1}{\operatorname{argmin}} \frac{1}{2}(y_\phi - \tilde{U}_1\xi_1)^T C_{y_\phi}^{-1}(y_\phi - \tilde{U}_1\xi_1) \\ &= \underbrace{(\tilde{U}_1^T C_{y_\phi}^{-1}\tilde{U}_1)^{-1}\tilde{U}_1^T C_{y_\phi}^{-1}}_{=:\tilde{U}_1^\dagger} y_\phi \end{aligned} \tag{3.8}$$

where $C_{y_\phi} := \tilde{U}_2 C_{\xi_2}\tilde{U}_2^T + C_\nu \in \Re^{m\times m}$ and $\tilde{U}_1^\dagger \in \Re^{r\times m}$ is generalized inverse satisfying $\tilde{U}_1\tilde{U}_1^\dagger\tilde{U}_1 = \tilde{U}_1$. Utilizing linearization relationship from (3.1) and estimated dominant state from (3.8), we have reconstruction of output measurement $y_\psi(t) \in \Re^s$ with reduced dominant state as

$$y_\psi(t) = \hat{S}U_1\hat{\xi}_1(t) = \hat{S}U_1\tilde{U}_1^\dagger y_\phi \tag{3.9}$$

Then, error and covariance of the reconstructed output measurement are given by

$$\begin{aligned} e_{y_\psi} &:= \tilde{\psi}(t) - y_\psi(t) \\ &= \hat{S}\tilde{\phi} - \hat{S}U_1\tilde{U}_1^\dagger(H\tilde{\phi} + \nu) \\ &= \underbrace{(\hat{S} - \hat{S}U_1\tilde{U}_1^\dagger H\ )}_{=:M_\phi}\tilde{\phi} - \underbrace{\hat{S}U_1\tilde{U}_1^\dagger}_{=:M_\nu}\nu \\ C_{e_{y\psi}} &= M_\phi C_\phi M_\phi^T + M_\nu C_\nu M_\nu^T \end{aligned}$$

With the information of the prior distribution of the state from (3.2) and linear relationship between the state and the output from (3.1), we have prior distribution of the output as follows:

$$\tilde{\psi}(t) \sim \mathcal{N}(0, C_\psi), \quad C_\psi := \hat{S} C_\phi \hat{S}^T \tag{3.10}$$

Now, utilizing the prior distribution (3.10) and reconstructed measurement (3.9), optimal output estimation is obtained with maximum a posteriori estimation

$$\begin{aligned}
\hat{\tilde{\psi}} &= \underset{\tilde{\psi}}{\operatorname{argmax}}\, p(\tilde{\psi}|y_\psi) \qquad (3.11)\\
&= \underset{\tilde{\psi}}{\operatorname{argmax}}\, p(y_\psi|\tilde{\psi}) p(\tilde{\psi}) \\
&= \underset{\tilde{\psi}}{\operatorname{argmax}}\, \frac{1}{\sqrt{(2\pi)^{2s}|C_{e_{y\psi}}||C_\psi|}} \exp\left[-\frac{1}{2}(y_\psi - \tilde{\psi})^T C_{e_{y\psi}}^{-1}(y_\psi - \tilde{\psi}) - \frac{1}{2}\tilde{\psi}^T C_\psi^{-1}\tilde{\psi}\right] \\
&= \underset{\tilde{\psi}}{\operatorname{argmin}}\, \frac{1}{2}(y_\psi - \tilde{\psi})^T C_{e_{y\psi}}^{-1}(y_\psi - \tilde{\psi}) + \frac{1}{2}\tilde{\psi}^T C_\psi^{-1}\tilde{\psi} \\
&= (C_{e_{y\psi}}^{-1} + C_\psi^{-1})^{-1} C_{e_{y\psi}}^{-1} y_\psi \qquad (3.12)
\end{aligned}$$

See Fig. 3.1, which illustrates the MAP estimation of the output. Note that if we choose $\hat{S} = I_{3n\times 3n}$, where $I_{3n\times 3n} \in \Re^{3n\times 3n}$ is identity matrix, we have estimation of the state itself.

3.2 Sensor Placement Optimization

Given limited number of sensors due to practical feasibility, decision of sensor placement is necessary. With the information of covariance of the output estimation error, we can optimize the sensor placement that minimizes the trace of the error covariance. From, (3.1), (3.7), (3.9), and (3.11), the output estimation error is given by

$$\begin{aligned} e_\psi(t) &:= \tilde{\psi} - \hat{\tilde{\psi}} \\ &= \hat{S}\tilde{\phi} - (C_{e_{y\psi}}^{-1} + C_\psi^{-1})^{-1} C_{e_{y\psi}}^{-1} y_\psi \\ &= \hat{S}\tilde{\phi} - (C_{e_{y\psi}}^{-1} + C_\psi^{-1})^{-1} C_{e_{y\psi}}^{-1} \hat{S} U_1 \tilde{U}_1^\dagger (H\tilde{\phi} + \nu) \\ &= \underbrace{\left[\hat{S} - (C_{e_{y\psi}}^{-1} + C_\psi^{-1})^{-1} C_{e_{y\psi}}^{-1} \hat{S} U_1 \tilde{U}_1^\dagger H\right]}_{=:M'_\phi} \tilde{\phi} - \underbrace{(C_{e_{y\psi}}^{-1} + C_\psi^{-1})^{-1} C_{e_{y\psi}}^{-1} \hat{S} U_1 \tilde{U}_1^\dagger}_{=:M'_\nu} \nu \end{aligned}$$

Consequently, covariance of e_ψ is given by

$$C_{e_\psi} = M'_\phi C_\phi M_\phi^{'T} + M'_\nu C_\nu M_\nu^{'T} \tag{3.13}$$

Note that C_{e_ψ} is function of sensor placement matrix H. Therefore, the optimal sensor placement matrix $H^* \in \Re^{m \times 3n}$ can be obtained such that minimizes the

trace of the estimation error covariance C_{e_ψ} as follows:

$$\begin{aligned} H^* &= \underset{H}{\operatorname{argmin}}\, \mathbf{tr}(C_{e_\psi}) \\ &= \underset{H}{\operatorname{argmin}}\, \mathbf{tr}\left[M'_\phi C_\phi M_\phi^{'T} + M'_\nu C_\nu M_\nu^{'T}\right] \\ &\quad \text{subj. to } H \in \Omega \end{aligned} \tag{3.14}$$

where Ω is defined as set of all possible H with limited number of sensors and practical feasibility. $\mathbf{tr}(\cdot)$ denotes trace of a matrix.

Chapter 4

Experiments

4.1 Testbed

4.1.1 Setup

We verified our estimation framework proposed in Chapter 3 via experiments. We designed EKC testbed with aluminum profiles of cross-section dimension 2cm×2cm. The system is constructed as six-link three-dimensional EKC. See Fig. 4.1. Each length of the link is 25cm and total height is 1.64m, which is about the height of a person. Links are connected with other short aluminum profiles and brackets. The testbed has desirable properties for EKC. However we tighten the connection between adjoining links, little gaps generated from

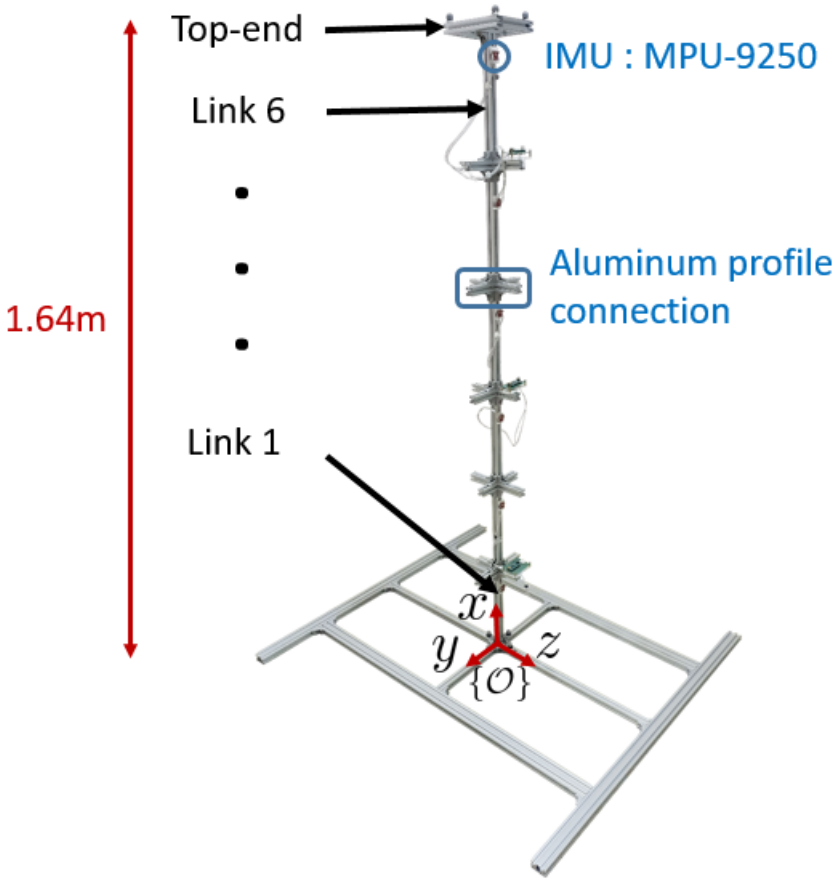

FIGURE 4.1: Six-link three-dimensional EKC testbed designed with aluminum profiles.

dimension of tolerance are unavoidable. Therefore they act as universal joints with stiff elastic components, which are the key properties of EKC we mentioned in Chapter 2.1. Links are numbered from 1 to 6 starting from bottom to top.

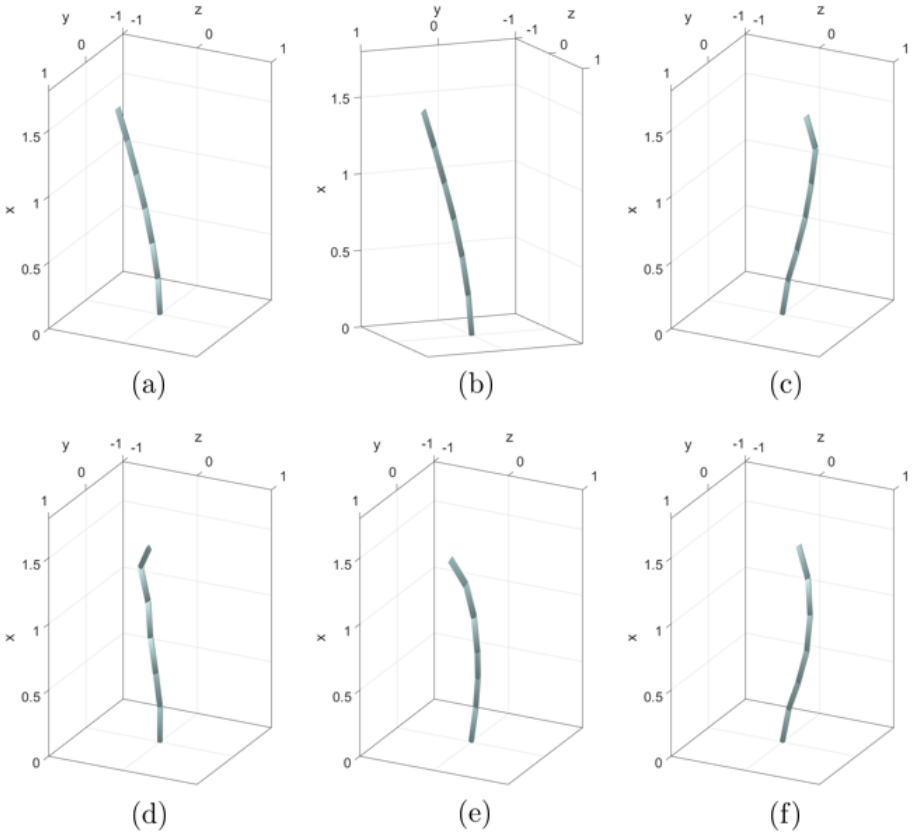

FIGURE 4.2: First six dominant mode shapes of the testbed. (a) mode 1, (b) mode 2, (c) mode 3, (d) mode 4, (e) mode 5, (f) mode 6.

For IMU, we use InvenSense MPU-9250, which is one of the commonly-used low-cost IMU. We have chosen this sensor because it is 9-axis IMU, so it can measure not only pitch (β), yaw (γ) of each link, but also roll (α) with magnetometer. We implemented explicit nonlinear complementary filter [7] to obtain the Euler angles of the links. Also, since we need 6 IMUs to be deployed on every link of

our testbed to obtain state covariance and apply POD in (3.2), low-cost IMUs were suitable.

In addition, we utilize OptiTrack, a motion capture system, to measure ground-truth value of our output $\tilde{\psi}(t)$, top-end motion, to verify performance of our framework. It is also used to calculate state-output linear relationship matrix $\hat{S}$ by regression as mentioned in (3.1).

Since the testbed is six-link EKC system, the dimension of the state is $\tilde{\phi}(t) \in \Re^{18}$. We are interested in top-end motion of the system, which is important factor for control of dual-arm height operation telerobotic system in [1]. For this reason, we choose the output $\tilde{\psi}(t) = [\tilde{\psi}_y(t), \tilde{\psi}_z(t)]^T \in \Re^2$, where $\tilde{\psi}_y(t)$ and $\tilde{\psi}_z(t)$, respectively, are top-end position deviation from its steady-state along y-axis and z-axis w.r.t. global frame $\{\mathcal{O}\}$ in Fig. 4.1.

4.1.2 Output Estimation Result

To obtain the state data samples as mentioned in (3.2), we applied external force at the top-end along y-axis and z-axis. Then, applying POD, we obtained singular values of C_ϕ as shown in Table 4.1. We set our threshold of $\frac{\sum_{i=1}^{r}\sigma_i}{\sum_{i=1}^{3n}\sigma_i}$ to be larger than 0.95. Therefore, we choose $r = 6$, which makes the ratio 0.989. First six dominant mode shapes (i.e., first six columns of U in (3.2)) are shown in Fig. 4.2. Since each IMU gives three measurements (i.e., roll, pitch, yaw of the attached link), we determined to use two IMUs, which give us equal number of

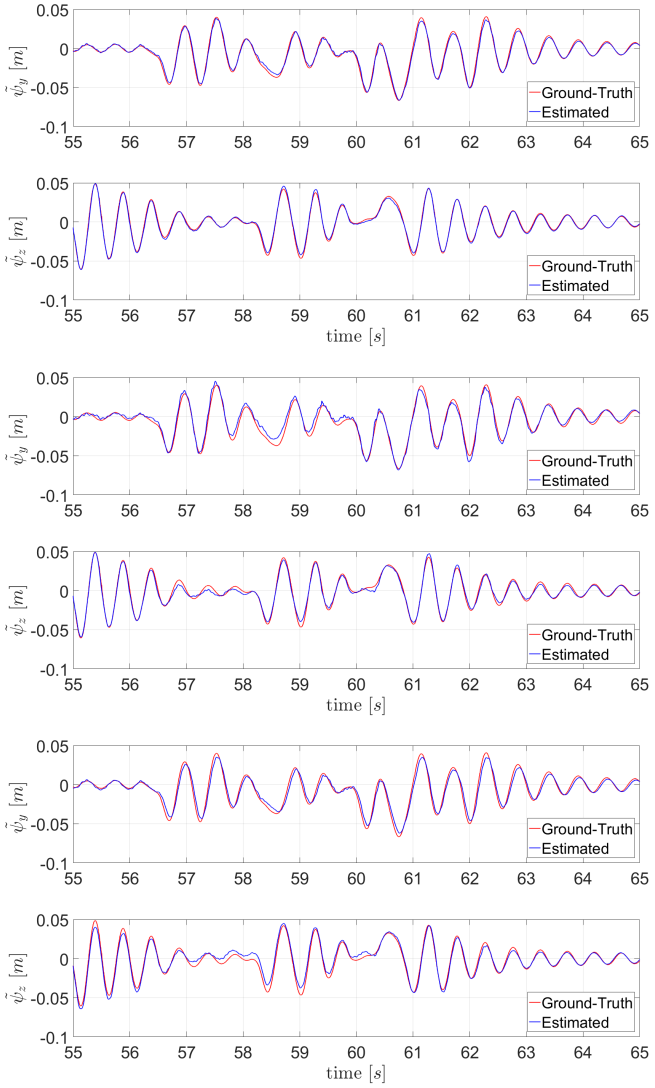

FIGURE 4.3: Testbed output estimation performance of three cases with least $\mathbf{tr}(C_{e_\psi})$: IMUs on link 1, 2 (top), IMUs on link 1, 3 (middle), IMUs on link 2, 4 (bottom).

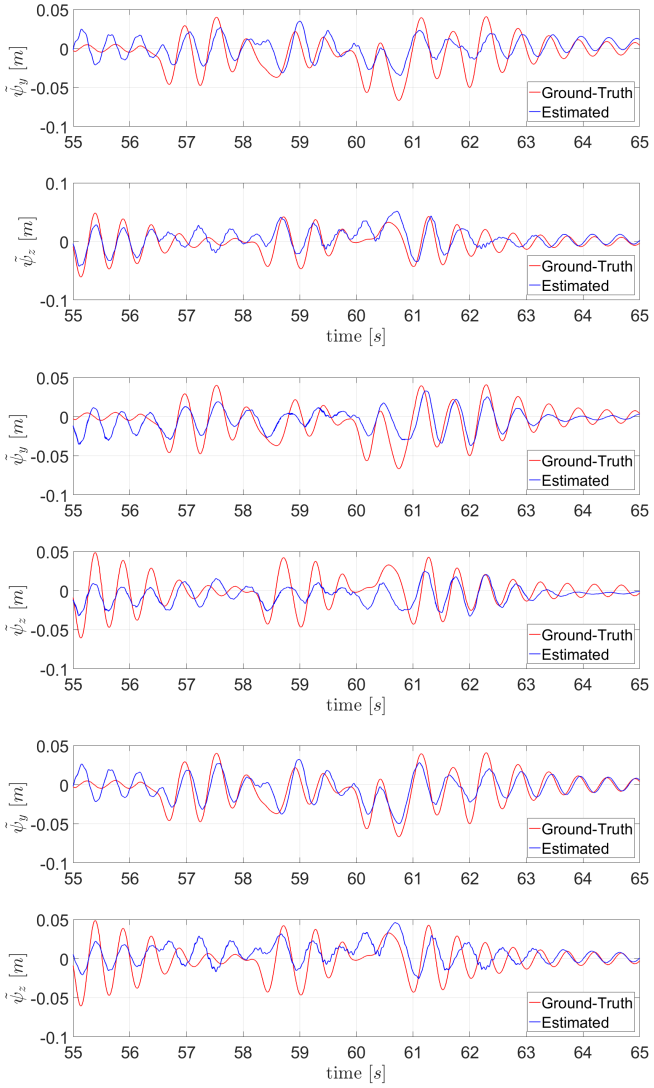

FIGURE 4.4: Testbed output estimation performance of three cases with greatest $\mathbf{tr}(C_{e_\psi})$: IMUs on link 3, 4 (top), IMUs on link 4, 5 (middle), IMUs on link 4, 6 (bottom).

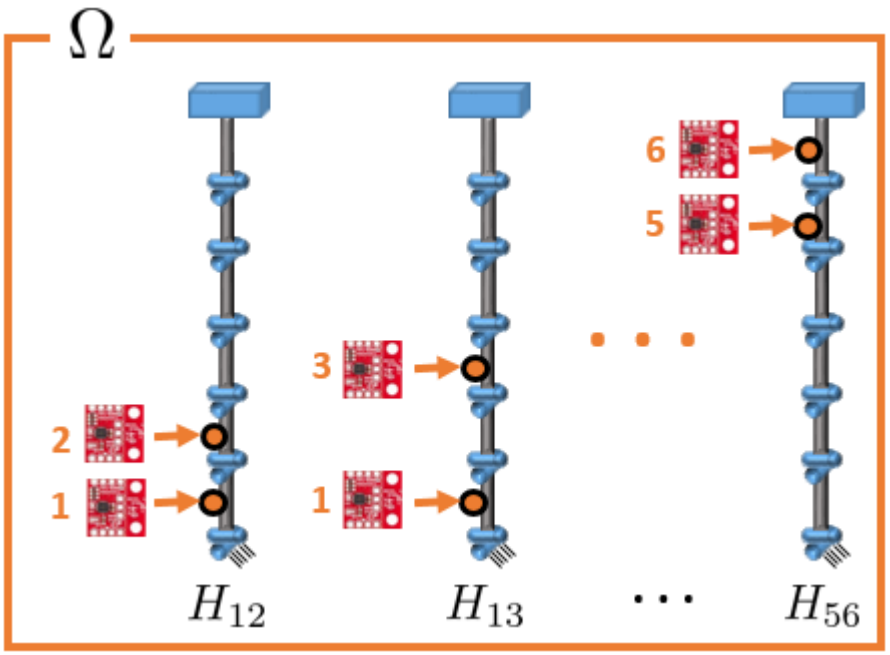

FIGURE 4.5: Set of all possible sensor placement matrices for six-link EKC.

measurements to the dimension of the reduced state $r = 6$. Therefore, possible set of IMU placement matrix Ω defined in Chapter 3.2 have fifteen elements, i.e., $\Omega = \{H_{12},\ H_{13},\ H_{14}, \cdots,\ H_{45},\ H_{46},\ H_{56}\}$. $H_{ij} \in \Re^{6\times 18}$ denotes the sensor placement matrix corresponding to the measurement matrix when IMUs are located at i-th link and j-th link as shown in Fig. 4.5. For example, H_{12} is

$$H_{12} = \begin{bmatrix} I_{3\times3} & 0_{3\times3} & 0_{3\times3} & 0_{3\times3} & 0_{3\times3} & 0_{3\times3} \\ 0_{3\times3} & I_{3\times3} & 0_{3\times3} & 0_{3\times3} & 0_{3\times3} & 0_{3\times3} \end{bmatrix}$$

σ_1	σ_2	σ_3
7.365×10^{-4}	6.046×10^{-4}	6.146×10^{-5}
σ_4	σ_5	σ_6
3.571×10^{-5}	2.233×10^{-5}	1.268×10^{-5}
σ_7	σ_8	σ_9
9.055×10^{-6}	3.717×10^{-6}	1.840×10^{-6}
σ_{10}	σ_{11}	σ_{12}
9.903×10^{-7}	5.590×10^{-7}	3.770×10^{-7}
σ_{13}	σ_{14}	σ_{15}
2.092×10^{-7}	1.079×10^{-7}	8.429×10^{-8}
σ_{16}	σ_{17}	σ_{18}
5.342×10^{-8}	2.951×10^{-8}	2.192×10^{-8}

TABLE 4.1: Testbed singular values of C_ϕ obtained from POD (diagonal elements of Σ)

To verify the performance of our proposed estimator (3.11), we applied random external force on y and z direction at the system top-end. Then, we compared estimated output to the ground-truth value obtained from motion capture system. See Fig. 4.3 and Fig. 4.4. RMS of output estimation error norm $\|e_\psi\|_2$ and trace of its covariance (3.13) for each IMU placement is listed in the Table 4.2.

Note that as we could predict from sensor placement optimization (3.14), RMS of the output estimation error norm is the smallest for case 1 in Table 4.2, which is the case with smallest $\mathbf{tr}(C_{e_\psi})$. On the other hand, the bad cases (RMS over 10 mm) also could be predicted from (3.14), where $\mathbf{tr}(C_{e_\psi})$ are the greatest.

Case	**IMU Loc.**	**RMS**($\|e_\psi\|_2$)	**tr**(C_{e_ψ})
1	1, 2	2.330 mm	4.252×10^{-6}
2	1, 3	3.352 mm	1.775×10^{-5}
3	1, 4	4.761 mm	3.690×10^{-5}
4	1, 5	4.136 mm	2.024×10^{-5}
5	1, 6	8.381 mm	7.934×10^{-5}
6	2, 3	7.196 mm	3.874×10^{-5}
7	2, 4	3.977 mm	1.430×10^{-5}
8	2, 5	5.051 mm	2.080×10^{-5}
9	2, 6	5.862 mm	3.194×10^{-5}
10	3, 4	15.20 mm	2.136×10^{-4}
11	3, 5	15.54 mm	2.117×10^{-4}
12	3, 6	13.19 mm	1.749×10^{-4}
13	4, 5	15.54 mm	2.596×10^{-4}
14	4, 6	14.70 mm	2.273×10^{-4}
15	5, 6	14.05 mm	1.612×10^{-4}

TABLE 4.2: Testbed RMS of output estimation error and trace of its covariance. Case 1 has the least RMS, which can be predicted from its trace of output estimation error covariance

4.2 Mock-up

4.2.1 Setup

Furthermore, we conducted experiment on six-link EKC mock-up as shown in Fig. 4.6. Length of each link is 0.815m, and total height is about 6m including

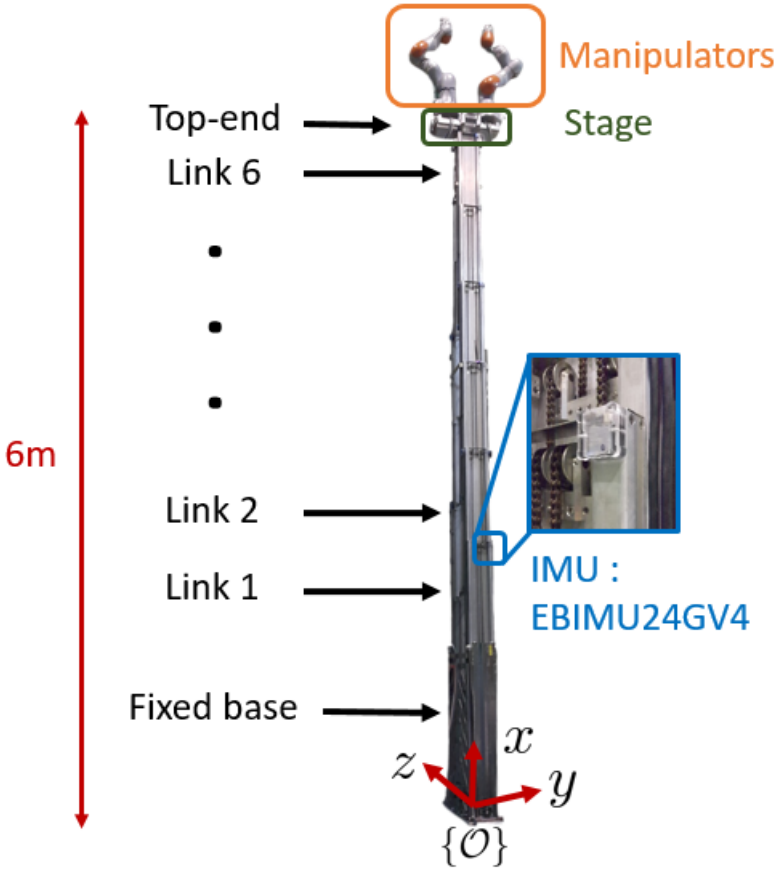

FIGURE 4.6: Six-link three-dimensional large-size EKC mock-up.

the fixed base. Also, two manipulators and one stage are placed on top-end of the mock-up.

E2Box EBIMU24GV4 wireless IMUs are used for measurement of the Euler

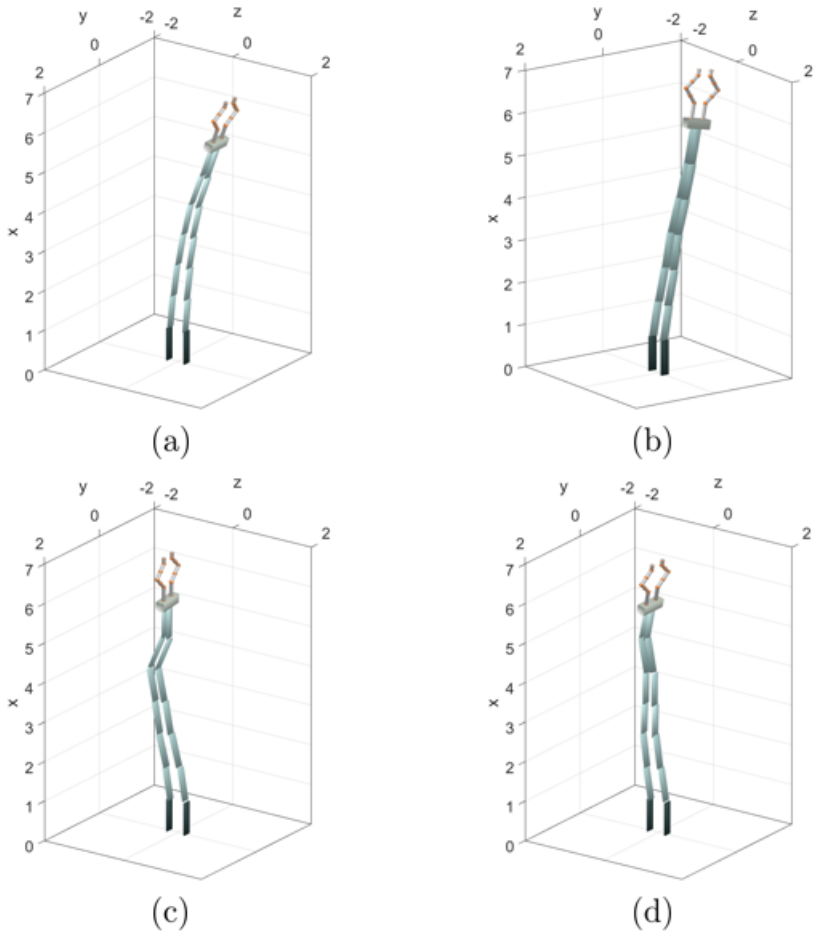

FIGURE 4.7: First four dominant modes of mock-up. (a) mode 1, (b) mode 2, (c) mode 3, (d) mode 4.

angles. Wireless IMUs were more convenient to deploy on the large-size mock-up than the wired ones. Unlike small-scale testbed, utilizing magnetometer to obtain roll (α) was infeasible for the large-size mock-up because magnetometer

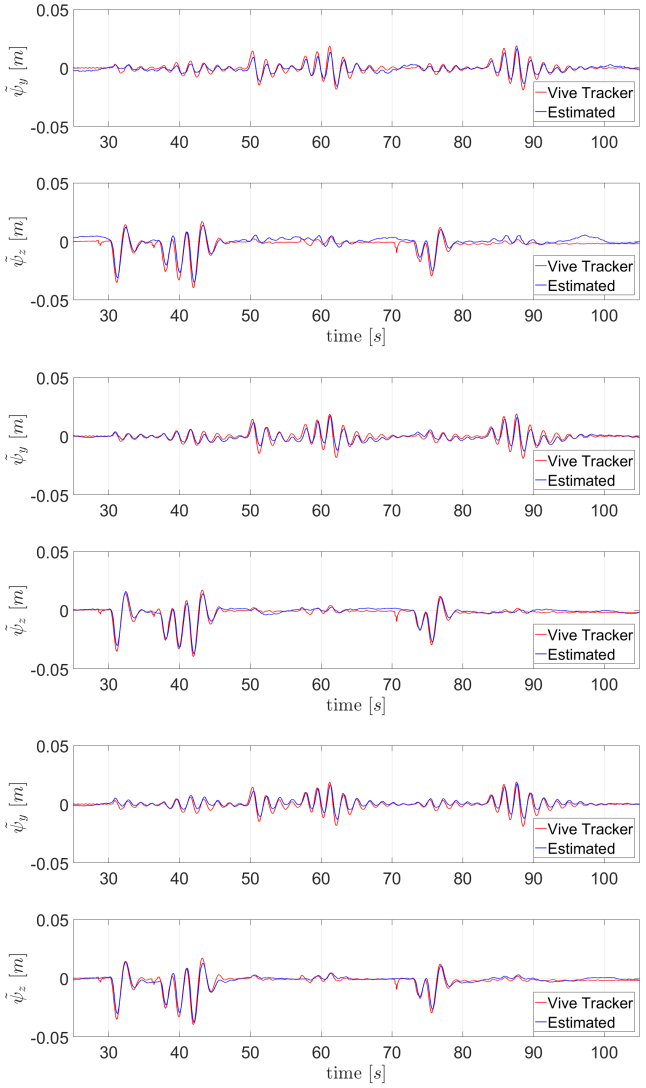

FIGURE 4.8: Mock-up output estimation performance of three cases with least $\mathbf{tr}(C_{e_\psi})$: IMUs on link 1, 6 (top), IMUs on link 3, 5 (middle), IMUs on link 4, 5 (bottom).

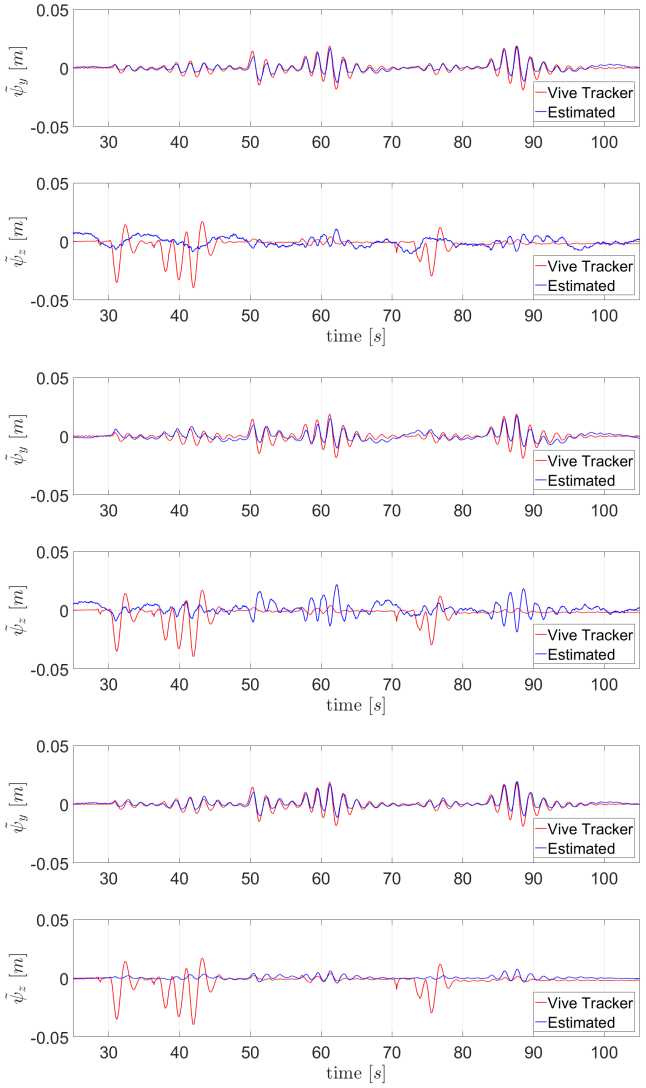

FIGURE 4.9: Mock-up output estimation performance of three cases with greatest $\mathbf{tr}(C_{e_\psi})$: IMUs on link 1, 2 (top), IMUs on link 1, 3 (middle), IMUs on link 2, 4 (bottom).

data became inaccurate due to its harsh environment and metallic, electronic components near the sensors. However, roll values can be considered zero around the steady-state. Since the EKC is modeled with universal joints, the state of the system $\tilde{\phi} \in \Re^{18}$ and the relative joint angles $q \in \Re^{12}$ have following linearized relation around steady-state

$$\tilde{\phi} \approx \left.\frac{\partial \phi}{\partial q}\right|_{q_{ss}} \tilde{q}$$

where $\tilde{q} := q - q_{ss} \in \Re^{12}$ is relative joint angle deviation from its steady-state. The mock-up has steady-state $q_{ss} = 0$, which implies

$$\left.\frac{\partial \phi}{\partial q}\right|_{q_{ss}=0} = \begin{bmatrix} M & 0_{3\times2} & 0_{3\times2} & 0_{3\times2} & 0_{3\times2} & 0_{3\times2} \\ M & M & 0_{3\times2} & 0_{3\times2} & 0_{3\times2} & 0_{3\times2} \\ M & M & M & 0_{3\times2} & 0_{3\times2} & 0_{3\times2} \\ M & M & M & M & 0_{3\times2} & 0_{3\times2} \\ M & M & M & M & M & 0_{3\times2} \\ M & M & M & M & M & M \end{bmatrix} \in \Re^{18\times12}$$

where

$$M := \begin{bmatrix} 0 & 0 \\ 1 & 0 \\ 0 & 1 \end{bmatrix} \in \Re^{3\times2}$$

Therefore it is straightforward to have following linearized approximation around the zero steady-state assuming small deviation of $\tilde{q}$

$$\tilde{\phi}_i = \begin{bmatrix} \tilde{\alpha}_i \\ \tilde{\beta}_i \\ \tilde{\gamma}_i \end{bmatrix} \approx \begin{bmatrix} 0 \\ \sum_{j=1}^{i} \tilde{q}_{2j-1} \\ \sum_{j=1}^{i} \tilde{q}_{2j} \end{bmatrix} \quad \text{for} \quad i = 1, \cdots, 6 \tag{4.1}$$

which implies magnetometers are not needed to measure roll value since it can be approximated as zero.

HTC Vive was used to measure top-end motion of the mock-up in alternative of OptiTrack, because OptiTrack system was infeasible to be installed at such harsh environment. HTC Vive only requires a base station and a tracker to obtain position value. Considering the zero steady-state $\phi_{ss} = 0$, from (3.1), we have

$$\hat{S} := \left.\frac{\partial h}{\partial \phi}\right|_{\phi_{ss}} = \begin{bmatrix} 0 & 0 & l_1 & \cdots & 0 & 0 & l_6 \\ 0 & -l_1 & 0 & \cdots & 0 & -l_6 & 0 \end{bmatrix} \in \Re^{2\times 18}$$

where l_i denotes length of i-th link.

4.2.2 Output Estimation Result

Similar to the testbed experiment, we applied external force at the top-end along y-axis and z-axis of the mock-up to obtain singular values of C_ϕ via POD as shown in Table 4.3. In addition, $\sigma_{13}, \cdots, \sigma_{18} = 0$, because we assumed roll values

zero from (4.1). We set our threshold of $\frac{\sum_{i=1}^{r}\sigma_i}{\sum_{i=1}^{3n}\sigma_i}$ to be larger than 0.95. Therefore, we choose $r = 4$, which makes the ratio 0.987. First four dominant modes are depicted in Fig. 4.7. Without magnetometer, IMU gives two measurements (i.e., pitch, yaw of the attached link), therefore we determined to use two IMUs, which give us equal number of measurements as number of the dominant modes $r = 4$. Hence possible set of IMU placement matrix Ω is defined same as that in Chapter 4.1.2, except that now the dimension of the sensor placement matrix $H \in \Re^{4\times 18}$ with measurement of only pitch and yaw from each IMU.

We applied external force on top-end of the mock-up, and compared our proposed estimation result with HTC Vive as shown in Fig. 4.8 and Fig. 4.9. RMS of the output estimation error norm $\|e_\psi\|_2$ and trace of its covariance for each IMU location is listed in Table 4.4. As we could predict from sensor placement optimization (3.14), case 11, 13 have the best performance with RMS under 3mm. On the other hand, case 1, 2, 4, 6, 7, 10 have poor performance with RMS over 7mm, which also could be predicted from our sensor placement optimization algorithm.

σ_1	σ_2	σ_3
6.906×10^{-5}	6.975×10^{-6}	2.639×10^{-6}
σ_4	σ_5	σ_6
9.353×10^{-7}	4.368×10^{-7}	2.386×10^{-7}
σ_7	σ_8	σ_9
1.575×10^{-7}	7.614×10^{-8}	5.742×10^{-8}
σ_{10}	σ_{11}	σ_{12}
3.977×10^{-8}	3.112×10^{-8}	1.399×10^{-8}

TABLE 4.3: Mock-up singular values of C_ϕ obtained from POD (diagonal elements of Σ)

Case	**IMU Loc.**	**RMS**($\|e_\psi\|_2$)	**tr**(C_{e_ψ})
1	1, 2	8.012 mm	1.967 $\times 10^{-4}$
2	1, 3	8.570 mm	1.624 $\times 10^{-4}$
3	1, 4	6.528 mm	3.536 $\times 10^{-5}$
4	1, 5	8.270 mm	4.293 $\times 10^{-5}$
5	1, 6	3.678 mm	7.491 $\times 10^{-6}$
6	2, 3	9.914 mm	1.146 $\times 10^{-4}$
7	2, 4	7.138 mm	2.273 $\times 10^{-4}$
8	2, 5	6.417 mm	3.056 $\times 10^{-5}$
9	2, 6	3.663 mm	1.387 $\times 10^{-5}$
10	3, 4	7.437 mm	5.868 $\times 10^{-5}$
11	3, 5	2.822 mm	4.050 $\times 10^{-6}$
12	3, 6	4.928 mm	1.322 $\times 10^{-5}$
13	4, 5	2.829 mm	2.668 $\times 10^{-6}$
14	4, 6	4.054 mm	1.466 $\times 10^{-5}$
15	5, 6	3.625 mm	1.018 $\times 10^{-5}$

TABLE 4.4: Mock-up RMS of output estimation error and trace of its covariance. The two cases (11, 13) with RMS under 3mm have the least **tr**(C_{e_ψ}). On the other hand, six cases (1, 2, 4, 6, 7, 10) with RMS over 7mm have the greatest **tr**(C_{e_ψ}).

Chapter 5

Conclusion and Future Work

5.1 Conclusion

In this thesis, we proposed a novel framework of model-free output estimation for high-DOF EKC (elastic kinematic chain) with limited number of sensors. Dominant modes of the system are obtained via POD (proper orthogonal decomposition) with richly excited state data. Thanks to mode reduction, we could choose minimum number of sensors to reconstruct measurement of user-defined output (e.g., top-end motion). Then, with the measurement and the prior probability of the output, we could apply maximum a posteriori (MAP) estimation to obtain optimal estimation. We could also analyze optimal sensor placement that minimizes the trace of the output estimation error covariance. Then, we

verified our framework with six-link three-dimensional small-scale EKC testbed and large-size mock-up.

5.2 Future Work

Future work includes the verification through the experiment of EKC system with higher DOF (i.e., more than six-link system). Although we focused on EKC system and IMU sensors because of simplicity, our framework can also be used for other similar setups, where each joint is connected by elastic components. Also, various sensors (e.g., camera, LiDAR, etc.) could be included to our framework. In addition, linear approximation around the steady-state could be relaxed if we apply some nonlinear techniques, however we spare it for the future research.

Bibliography

[1] C. Ha, H. Kim, and D. Lee. Passivity-based control of manipulator-stage systems on vertical flexible beam. In *Proc. IEEE/RSJ Int'l Conference on Intelligent Robots and Systems*, pages 429–435, 2017.

[2] G. Kerschen, J. C. Golinval, A. F. Vakakis, and L. A. Bergman. The method of proper orthogonal decomposition for dynamical characterization and order reduction of mechanical systems: an overview. *Nonlinear Dynamics*, 41 (1-3):147–169, 2005.

[3] K. Willcox and J. Peraire. Balanced model reduction via the proper orthogonal decomposition. *AIAA Journal*, 40(11):2323–2330, 2002.

[4] S. M. Kay. *Fundamentals of statistical signal processing, volume I: estimation theory.* Prentice Hall, 1993.

[5] T. Bretl and Z. McCarthy. Mechanics and quasi-static manipulation of planar elastic kinematic chains. *IEEE Transactions on Robotics*, 29(1):1–14, 2013.

[6] Y. Lee, M. Kim, Y. Lee, J. Kwon, Y. L. Park, and D. Lee. Wearable finger tracking and cutaneous haptic interface with soft sensors for multi-fingered virtual manipulation. *IEEE/ASME Transactions on Mechatronics*, 2018 (Accepted).

[7] R. Mahony, T. Hamel, and J. M. Pflimlin. Nonlinear complementary filters on the special orthogonal group. *IEEE Transactions on Automatic Control*, 53(5):1203–1218, 2008.

[8] J. Burgner-Kahrs, D. C. Rucker, and H. Choset. Continuum robots for medical applications: A survey. *IEEE Transactions on Robotics*, 31(6):1261–1280, 2015.

[9] M. W. Hannan and I. D. Walker. Real-time shape estimation for continuum robots using vision. *Robotica*, 23(5):645–651, 2005.

[10] A. Borum, D. Matthews, and T. Bretl. State estimation and tracking of deforming planar elastic rods. In *Proc. IEEE Int'l Conference on Robotics and Automation*, pages 4127–4132, 2014.

[11] E. J. Lobaton, J. Fu, L. G. Torres, and R. Alterovitz. Continuous shape estimation of continuum robots using x-ray images. In *Proc. IEEE Int'l Conference on Robotics and Automation*, pages 725–732, 2013.

[12] J. Jeon and B. Yi. Shape prediction algorithm for flexible endoscope. In *Proc. IEEE Int'l Conference on Robotics and Automation*, pages 2856–2861, 2014.

[13] S. C. Ryu and P. E. Dupont. Fbg-based shape sensing tubes for continuum robots. In *Proc. IEEE Int'l Conference on Robotics and Automation*, pages 3531–3537, 2014.

[14] R. J. Roesthuis, M. Kemp, J. J. van den Dobbelsteen, and S. Misra. Three-dimensional needle shape reconstruction using an array of fiber bragg grating sensors. *IEEE/ASME Transactions on Mechatronics*, 19(4):1115–1126, 2014.

[15] J. Ahn, J. Yoon, J. Lee, and D. Lee. Model-free optimal estimation and sensor placement framework for elastic kinematic chain. In *Proc. IEEE Int'l Conference on Robotics and Automation*, 2019 (Submitted).

[16] I. T. Jolliffe. *Principal component analysis*. Springer-Verlag, 2002.

[17] T. Kim. Frequency-domain karhunen-loeve method and its application to linear dynamic systems. *AIAA Journal*, 36(11):2117–2123, 1998.

[18] B. Moore. Principal component analysis in linear systems: Controllability, observability, and model reduction. *IEEE Transactions on Automatic Control*, 26(1):17–32, 1981.

[19] S. Lall, J. E. Marsden, and S. Glavaški. A subspace approach to balanced truncation for model reduction of nonlinear control systems. *Int'l Journal of Robust and Nonlinear Control*, 12(6):519–535, 2002.

[20] S. Lall, J. E. Marsden, and S. Glavaški. Empirical model reduction of controlled nonlinear systems. In *Proc. IFAC World Congress*, pages 2598–2603, 1999.

요약

본 논문에서는 데이터기반 주성분분석 기법 및 최대 사후 확률 추정기법을 활용하여 제한된 개수의 관성센서만을 사용하는 고자유도 유연 시스템의 모델프리 최적 추정 및 센서 배치 최적화 프레임워크를 개발하였다. 우선, 사전에 유연 시스템을 대표적인 시나리오에 대하여 충분히 가진하여 얻은 데이터로부터 주성분분석을 적용시켜 우세 모드와 열세 모드로 분할하였다. 이렇게 구한 각 모드의 특이값을 기반으로 필요한 최소한의 관성센서 개수를 정할 수 있었으며 시스템 끝단의 위치와 같은 출력의 사전 분포를 구할 수 있었다. 출력의 사전 분포와 관성센서의 위치에 따른 최대 사후 확률 추정을 할 수 있었으며, 추정 성능을 최대화하기 위한 센서 배치 최적화기법 또한 제시하였다. 그리하여 최적화된 센서 배치로 유연 시스템의 실시간 출력 최적 추정이 가능하였다. 최종적으로 본 논문에서 제시한 추정 및 센서 배치 최적화 프레임워크를 실험을 통하여 검증하였다.

주요어: Elastic kinematic chain, Proper orthogonal decomposition, Proper orthogonal mode, Mode reduction, Maximum a posteriori estimation, Sensor placement optimization

학번: *2017-28758*